

Deep Learning based Extreme Heatwave Forecast

Valerian Jacques-Dumas, Francesco Ragone, Freddy Bouchet,
Pierre Borgnat *Member, IEEE*, Patrice Abry *Fellow, IEEE*

Abstract—Forecasting the occurrence of heatwaves constitutes a challenging issue, yet of major societal stake, because extreme events are not often observed and (very) costly to simulate from physics-driven numerical models. The present work aims to explore the use of Deep Learning architectures as alternative strategies to predict extreme heatwaves occurrences from a very limited amount of available relevant climate data. This implies addressing issues such as the aggregation of climate data of different natures, the class-size imbalance that is intrinsically associated with rare event prediction, and the potential benefits of transfer learning to address the nested nature of extreme events (naturally included in less extreme ones). Using 1000 years of state-of-the-art PlaSim Planete Simulator Climate Model data, it is shown that Convolutional Neural Network-based Deep Learning frameworks, with large-class undersampling and transfer learning achieve significant performance in forecasting the occurrence of extreme heatwaves, at three different levels of intensity, and as early as 15 days in advance from the restricted observation, for a single time (single snapshot) of only two spatial fields of climate data, surface temperature and geopotential height.

Index Terms—extreme event forecasting, heatwave forecasting, climate, deep learning, convolutional neural networks, transfer learning, class-size imbalance.

I. INTRODUCTION

Context: Climate extreme event impacts and forecast.

Climate change constitutes one of the major concerns of modern societies. Its most severe impacts are caused by rare and extreme events. For instance, recent decades witnessed a number of exceptionally warm summers and record breaking heatwaves [1]. At Northern hemisphere mid-latitudes, relevant such examples were observed over France and Western Europe in summer 2003, with a death toll of about 70,000 [2], or over Russia in summer 2010 [3], [4], with long lasting (several weeks) periods of anomalous heat. Because of their being rare, with return periods of (beyond) centuries, forecasting the occurrence of such events, estimating their occurrence probability or detecting early-precursors is a key challenge in climate sciences. The main methodological bottlenecks stem from both a lack of historical data and severe issues in heavy and costly simulating physics models over long enough periods of time to sample such rare events.

Related work: machine learning in climates sciences.

Machine learning has now been used for decades in climate and weather forecast sciences, with various goals such as post-processing, data assimilation, physical analysis,... Recently,

deep neural networks were used, with noticeable successes, for prediction purpose [5], [6], [7]. While deep learning based prediction performance remain far from challenging the prediction capabilities of physics modelling-driven procedures [5], they prove useful to improve physics models [8] or their parameter-tunings [9], [10], to complement them for analysis or pattern recognition [11], or to perform tasks not achievable with physics models. Machine learning has also been used for extreme weather event prediction [12] or severe weather risk assessment [13]. In [12], it is shown that the CapsNet deep neural network is a fast and efficient tool, for predicting hot days several days ahead.

While most past studies remain focused on intra-day extreme temperature event occurrence, long lasting heatwaves are the most impactful for health [3] and biodiversity. This is because the costs of long-term runs of full physics-driven models, required to sample rare events, preclude the accurate and timely assessment of long and extreme heatwaves. This would require ensemble simulations, i.e., repeating many independent simulations of the same phenomenon with different initializations. However, when using the best physics models, given their costs, such simulations are limited typically to a few tens of independent realizations at most, which is not suited for studying rare events. The prediction of long lasting extreme heatwaves thus constitutes a challenging technical issue and major societal stake, addressed here.

Goals, contributions and outline. The present work aims to propose deep learning based architectures to predict the occurrence of long-duration extreme heatwaves from realistic climate data, and to quantify their performance. The goal is not to replace the use of physics models but to complement them by performing specific tasks that they cannot achieve, such as, for example, forecasting the occurrence of extreme heatwaves from only a restricted subset of observed climate data, e.g., to the temperature field for a single day.

To that end, realistic climate data obtained from planet simulator climate model can be made available in reasonable size and at reasonable costs for deep learning architecture training. Data and productions conditions are described in detail in Section II, where the definition of extreme heatwaves is also provided.

Deep learning based heatwave prediction implies addressing a number of crucial methodological issues: i) propose a suitable deep learning architecture; ii) overcome the imbalance in class-sizes intrinsically associated with extreme events and requiring the use of sampling strategies; and iii) account for the nested nature of extreme events (most extreme events are included in less extreme ones) which suggests the potential use of transfer learning. These methodological issues are addressed

All authors are with Univ Lyon, Ens de Lyon, Univ. Claude Bernard, CNRS, Laboratoire de Physique, Lyon, France. Francesco Ragone is also with Earth and Life Institute, Université Catholique de Louvain, Louvain-la-neuve, Belgium, and Royal Meteorological Institute, Brussels, Belgium. e-mail: firstname.lastname@ens-lyon.fr. Work supported by the ACADEMICS Grant of IDEXLYON, Univ. Lyon, PIA ANR-16-IDEX-0005.

and discussed in Section III.

Results, reported in Section IV, first compare aggregation protocols aiming to best combine different available observations, and second discuss the benefits of using transfer learning in nested extreme events prediction strategies as well as non extreme event large class undersampling, (see Section IV-A).

Furthermore, the significant ability of Convolutional Neural Network-based Deep Learning architectures to perform relevant long-lasting (14 days) extreme (top few %) heatwave occurrence forecasting from reduced sets of climate data snapshots several days in advance is quantified (see Section IV-B). Notably, it is shown that the occurrence of heatwaves can be predicted up to $\tau = 15$ days in advance, thus significantly beyond typical correlations times for climate data of the order of 3 to 5 days [14].

II. CLIMATE DATA AND HEATWAVES

Climate model data. The data used in the present work are produced by the Planet Simulator (PlaSim) climate model [15], [16], [17]. Its dynamical core solves the primitive equations for vorticity, divergence, temperature and surface pressure. Moisture is included by transport of water vapor. The governing equations are solved using a spectral transform method. Unresolved processes, such as radiation, interactive clouds, moist and dry convection, large-scale precipitation, boundary layer fluxes of latent and sensible heat and vertical and horizontal diffusion are parametrized. The model also simulates the coupling with land surface scheme and ocean. The horizontal resolution is T42 in spectral space, corresponding to a spatial resolution of about 2.8 degrees in both latitude and longitude. In practice, the horizontal fields of data have a spatial size of 64×128 pixels, covering the entire globe. The vertical resolution corresponds to 10 vertical layers. The model is setup to run with fixed greenhouse gases concentrations and boundary conditions (incoming solar radiation and sea surface temperature and sea ice cover distributions) cyclically repeated every year, in order to generate a stationary state reproducing a climate close to the one of the 1990's. Thousands physical years of model outputs are available. They were computed on 16 processors and the total simulation took 1111 hours to compute.

Climate data and heatwaves. The present work focuses on predicting summer heatwaves. For that, two horizontal fields classically associated with heatwave mechanisms [17] are used only amongst the very large size PlaSim outputs: the surface temperature T_s in Kelvin and the height, in meters, of the geopotential on the isopressure surface of 500 hectoPascal (hPa), Z_g , located in the middle troposphere. The relation between surface temperature and heatwaves is straightforward. In weather and climate dynamics, the geopotential height in the middle of the troposphere is considered an excellent representation of the dynamical state of the atmosphere. Indeed, the geopotential height (in meters) at 500-hPa, Z_g is further tightly related to anticyclones (positive values) and cyclones (negative values) in the lower atmosphere. Moreover, to a good approximation, the wind flows along the isolines

of the geopotential height.

Heatwave definition. Let us precisely define heatwaves. For that, it is first needed to define temperature and geopotential height fluctuations, also called anomalies. Let $T_s(\vec{r}, t)$ denote the surface temperature at location \vec{r} and time index t , where time is counted independently from 0 for each year and sampled at a 3-hour resolution. The ensemble average $\langle T_s \rangle(\vec{r}, t)$ is obtained as the average across the 1000 years of $T_s(\vec{r}, t)$ for each given location \vec{r} and intra-year time t , thus preserving intra-year seasonal effect. The temperature fluctuation is further defined as $(T_s - \langle T_s \rangle)(\vec{r}, t)$. Geopotential height fluctuation is defined accordingly. A snapshot of maps of temperature and 500-hPa geopotential height fluctuations is shown in Fig. 1.

A heatwave, of duration D above an area \mathcal{A} and of strength a , is said to occur at time t , when the time-space average $Y(t)$ of the temperature fluctuations exceeds a threshold a :

$$Y(t) = \frac{1}{D} \int_t^{t+D} \frac{1}{\mathcal{A}} \int_{\mathcal{A}} (T_s - \langle T_s \rangle)(\vec{r}, u) d\vec{r} du > a.$$

For the present work, we study summer heatwaves (occurring in June, July, August only) over France ($\equiv \mathcal{A}$) lasting for $D = 14$ days.

By nature, heatwaves constitute rare events. We will consider three strength levels defined as the 5%, 2.5% or 1.25% most extreme events, yielding thresholds in time-space average of temperature fluctuations of, $a_5 = 3.08\text{K}$, $a_{2.5} = 3.7\text{K}$, and $a_{1.25} = 4.23\text{K}$.

Heatwave prediction dataset. For the prediction of heatwaves over France, data are restricted to dynamically relevant areas: North Hemisphere mid-latitudes, above 30°N , marked by the thick black box in Fig. 1, corresponding to fields of size 25×128 .

Because a direct use of data in the physical space would imply to handle spherical geometry and related boundary conditions, it has been chosen here to work with their spatial Fourier Transform (FT), computed on a 64×64 grid, with a frequency resolution of approximately $\delta F \simeq 10^{-4}\text{km}^{-1}$ in each direction.

The data used as inputs of the supervised learning procedure described in Section III below thus consist of couples (X_t, Z_t) , for t ranging from June 1st to August 31st, for 1000 years of simulation. Vector Z_t denotes a binary label, with value 1 when $Y(t) > a$, i.e., when there is an occurrence of heatwave in the next D -days, and 0 otherwise. X_t stands for the $64 \times 64 \times 2$ spatial FT \hat{T}_s and \hat{Z}_g of fields $T_s(t - 8 \times \tau)$, and $Z_g(t - 8 \times \tau)$, where τ denotes the delay (in days) between the date of observations and the date at which a prediction of heatwave occurrence is to be made (the factor 8 stems from the choice of the 3-hour sampling period for t). In other words, to make a prediction of heatwave occurring sometimes between today and the next D days, data observed τ days prior to today are used.

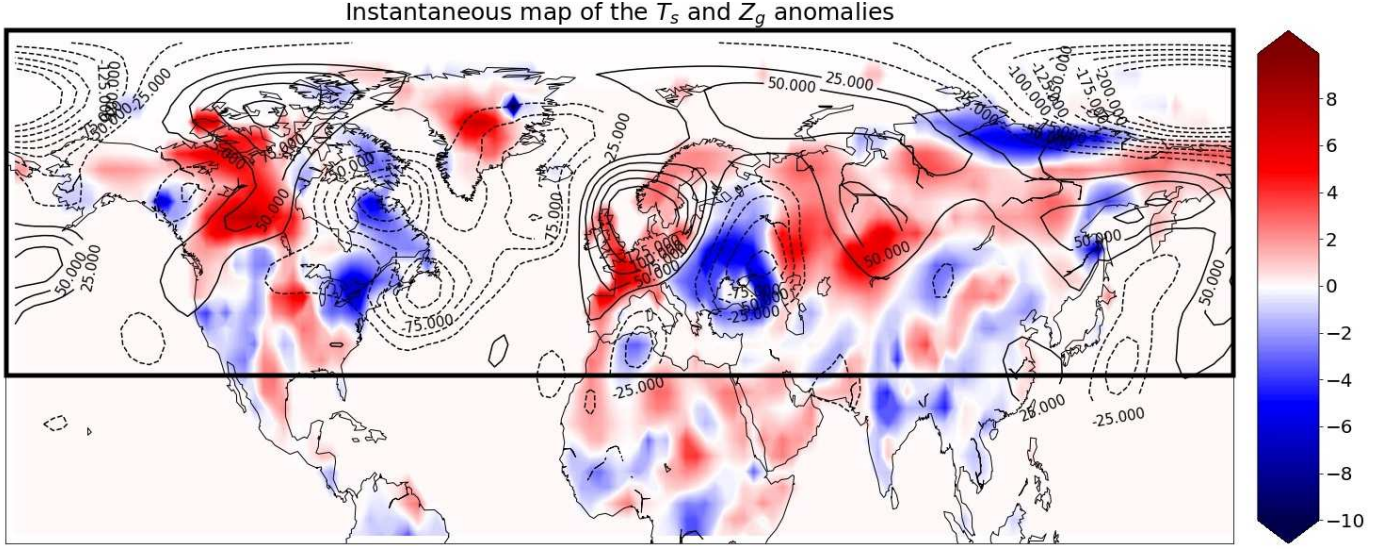


Fig. 1: Snapshot of the surface temperature surface fluctuations (T_s fluctuations, according to the color bar, in Kelvin) and of the geopotential height at 500mbar (Z_g fluctuations, contours) over the Northern Hemisphere. This snapshot is taken on July 20th on a arbitrary year of the PlaSim simulation. The spatial resolution is 64×128 (latitude \times longitude). The thin contour lines, representing the anomaly of Z_g , are in meters. The thick black contour delimitates the zone that is used for prediction by the machine learning procedure.

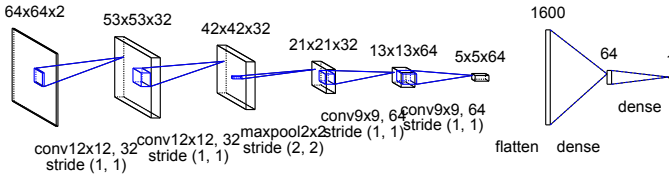


Fig. 2: CNN-based heatwave predictor architecture.

III. DEEP LEARNING ARCHITECTURES AND PROCEDURES

Convolutional Neural Network (CNN) architecture.

Heatwave prediction is performed using the CNN-based deep-learning 4 layer-architecture depicted in Fig. 2. The first two convolutional layers have filters of size 12×12 and ReLU activation functions. They are followed by a maxpool layer so as to divide data size by 2×2 with spatial dropout. The next two convolutional layers have filters of size 9×9 and ReLU activation functions and are also followed by a spatial dropout. Finally, a flatten operation and two fully connected layers followed by a sigmoid activation yield an output between $0 \leq q \leq 1$. This output is associated with the probability of occurrence of an heatwave in the upcoming D days. A heatwave is predicted then if the output q is above a threshold, set here to 0.5.

Train/test sets. Typical time scales governing climate dynamics permit to consider the 1000 year PlaSim simulation data as 1000 independent trajectories, yet with significant intra-year spatiotemporal dependencies, that can be exploited for heatwave detection. Therefore, the training set does not select events at random in time index and uniformly across the entire dataset. Instead, the train/test split is based on the random sampling of full years, with 900 such years associated

to the train set, while the test set comprises the 100 remaining years. The overall training set thus gathers $K = 648000$ samples ($900 \text{ years} \times 3 \text{ months} \times 30 \text{ days} \times 8 \text{ samples per day}$). Furthermore, train and test sets are also constructed to ensure that they contain, on average, the same percentages of rare events. It is an important aspect, as the objective is to detect rare events. We need to prevent imbalance of events between train and test sets.

Learning parameters. Learning architectures, training and testing are implemented using Python with Keras API. For optimization, Adam amsgrad variant is used, with a learning rate of $2 \cdot 10^{-4}$ and momentum of 0.5. The dropout rate is set to 30%. Batch size is set to 1000 samples. Batch normalization is applied after each layer. The number of training epochs¹ is set empirically to 10 when using the threshold a_5 , and to 5 for the two other thresholds $a_{2.5}$ and $a_{1.25}$. As the problem consists in detecting the absence or presence of heatwave (based on temperature anomaly), the loss function is the standard Binary Cross-Entropy, commonly used for classification tasks [18].

Class-size imbalance and undersampling. For the prediction of rare events, classes are imbalanced by construction. It has been well-documented that machine learning training is severely impaired by imbalanced class sizes [19], [20]. Here, we propose to handle this by *undersampling*: only a fraction of (randomly selected) non heatwave samples are used. A natural starting idea is to ensure, on average, equal sizes for both classes. This leads to subsample the non heatwave class by factors S_a of 1/19, 1/39 and 1/79, respectively

¹The number of epochs is the number of training iterations over the whole dataset, here the 900 years of the train set.

for the three heatwave levels $a_5, a_{2.5}$ and $a_{1.25}$. Less severe subsampling rates are also tested by considering multiplying by s the previous subsampling rates, with $s = 1, s = 2, s = 4$ and $s = 10$. This subsampling procedure yields training set of size $K_{a,s} = K \times p_a + K \times (1 - p_a) \times S_a \times s$, where $p_a = 0.05, 0.025, 0.0125$ corresponds to the fraction of most extreme events associated with threshold $a_5, a_{2.5}$ and $a_{1.25}$. For the higher heatwave levels, this reduces a lot the number of training samples. We propose a second approach based on Transfer learning to leverage the larger size of the available training set at lower level heatwaves.

Transfer learning. Heatwave detection is performed for three different intensity levels. The direct approach is to train the learning procedure for each of the three levels, independently and using random initialization: the weights are initialized using the Glorot uniform initializer [21]. A more elaborated second approach is proposed, using transfer learning [22] for the two highest levels, consisting in three steps: (i) learning is first performed for the 5% most extreme events, then (ii) learning for the top 2.5% is performed, using as initialization step the weights of the CNN learned for the 5% heatwave level. Further, (iii) learning for the top 1.25% is performed, using as initialization step the weights of the CNN learned for the 2.5% heatwave level. Of importance, to ensure meaningful statistical performance assessment, the same train set is used during learning for the three levels of heatwaves, both with and without transfer learning.

Performance assessment. To assess quantitatively the relevance of CNN-based heatwave occurrence prediction, the train/test procedure for the three levels of heatwaves, with and without transfer learning, is repeated 40 times, with independent train/test data split, respecting the procedure described above. For each of these 40 trials, detection performance is assessed by computing, on the test set, the rates (in percentage) of True Positives (TP), True Negatives (TN), False Positives (FP) and False Negatives (FN). The Matthews Correlation Coefficient (MCC) [23] is also reported, that is a single number score that balances the Type-I vs. Type-II errors (incorrect detection of a heatwave versus non detection when it occurs) and that accounts for imbalance between class sizes. Means, medians, standard deviations and maximum absolute deviations of these scores are computed by average across trials.

IV. HEATWAVE OCCURRENCE FORECASTING

A. Data aggregation, undersampling and transfer learning

To address the methodological issues of data aggregation, training set undersampling and transfer learning, analyses first concentrate on the easiest case $\tau = 0$. Let us emphasize however that predicting the occurrence of heatwave at $\tau = 0$ is far from trivial, as it implies predicting from data at time t , the existence of heatwaves occurring at any time between t and $t + D$.

Surface temperature versus geopotential height. As described in Section II, data available for heatwave predictions

consist of the $64 \times 64 \times 2$ spatial FT $\tilde{T}_s(t)$ and $\tilde{Z}_g(t)$ of $T_s(t)$ and $Z_g(t)$, respectively, for each time position t . Table I first compares forecasting performance from two independent learning protocols:

P1) T_s -only, using $\tilde{T}_s(t)$ alone as a $64 \times 64 \times 2$ tensor CNN input ;

P2) Z_g -only, using $\tilde{Z}_g(t)$ alone as a $64 \times 64 \times 2$ tensor CNN input.

Table I shows first that surface temperature and geopotential height independently contain enough spatial structures to predict heatwave occurrences, even for the most extreme events, with MCC that positively departs from 0. Table I however also clearly shows that surface temperature as input alone outperforms geopotential height as input alone in terms of MCC, and this all the more as the most extreme heatwaves are targeted. Interestingly, Table I further shows that the poorest performance of geopotential height comes from much higher rates of False Positives. This may come as no surprise since heatwaves are intrinsically defined in terms of surface temperature fluctuations.

Additionally, Table I shows that the rate of False Positives that are common between independent predictions from surface temperature and geopotential height are low. This suggests to combine these two independent detections to take advantage of the joint information available in these two fields. A naive and straightforward approach consists in performing a logical *AND* between the outputs of the two independent predictions. However, Table I indicates that the resulting MCC is not increased (with transfer learning) compared to that obtained from surface temperature only, and even decreased (without transfer learning), thus calling for more advanced data aggregation procedures.

Data aggregation. Two new learning protocols based on aggregation of surface temperature and geopotential height data, are proposed here. We defined them as:

P3) Combined- $T_s Z_g$, using both $\tilde{T}_s(t)$ and $\tilde{Z}_g(t)$, while using each of them as a $64 \times 64 \times 2$ tensor input of an independent CNN with same architecture as that described in Section III, but for the last fully-connected layer: the flattened outputs of both CNN are concatenated to serve as the input of a single final fully-connected layer;

P4) Stacked- $T_s Z_g$, using jointly $\tilde{T}_s(t)$ and $\tilde{Z}_g(t)$ by stacking them into a $64 \times 64 \times 4$ tensor used as the input of the CNN.

Table II reports the forecasting performance of these four protocols in terms of MCC (averages, medians and standard deviations obtained from 40 independent learning). Comparing Table I and Table II first strikingly shows that aggregation protocol P3 (Combined- $T_s Z_g$) only marginally outperforms the much simpler and less costly logical *AND* based combination of protocols P1 (T_s -only) and P2 (Z_g -only). Table II further clearly shows that aggregation protocol P4 (Stacked- $T_s Z_g$), combined with transfer learning, outperforms aggregation protocol P3 (Combined- $T_s Z_g$). This clearly indicates that the cross-spatial dynamics of surface temperature and geopotential height also contains relevant information pertaining to heatwave production

Without transfer learning	True Positives			False Positives			Average MCC		
	5%	2.5%	1.25%	5%	2.5%	1.25%	5%	2.5%	1.25%
Levels									
T_s alone	43.43%	39.70%	33.57%	5.18%	3.01%	2.34%	0.33	0.30	0.23
Z_g alone	56.29%	38.27%	22.67%	14.23%	10.34%	7.47%	0.25	0.14	0.06
Events in common	29.91%	18.70%	7.75%	2.11%	0.86%	0.32%	0.33	0.25	0.13
With transfer learning	True Positives			False Positives			Average MCC		
	5%	2.5%	1.25%	5%	2.5%	1.25%	5%	2.5%	1.25%
Levels									
T_s alone	—	30.43%	24.56%	—	2.03%	1.05%	—	0.27	0.23
Z_g alone	—	46.40%	38.40%	—	8.07%	5.15%	—	0.21	0.17
Events in common	—	19.39%	13.53%	—	0.70%	0.30%	—	0.27	0.22

TABLE I: **Compared performance for heatwave occurrence prediction from surface temperature vs. geopotential height.** Compared Percentage of True positive/False positive rates for prediction, for each heatwave levels (5%, 2.5% and 1.25%), with and without transfer learning, together with MCC. Average across 40 independent learning as described in Table II. The first two lines correspond to T_s alone and Z_g alone, while the last line quantifies a logical AND (i.e., joint prediction by T_s and Z_g). Percentages of True Positives (resp. False Positives) rates are quantified with respect to the sizes of the positive (resp. negative) class.

Without transfer learning	Stacked FT of T_s and Z_g			FT of T_s and FT of Z_g			FT of T_s alone			FT of Z_g alone		
	5%	2.5%	1.25%	5%	2.5%	1.25%	5%	2.5%	1.25%	5%	2.5%	1.25%
Average MCC	0.44	0.37	0.29	0.35	0.33	0.25	0.33	0.31	0.25	0.25	0.19	0.11
Median MCC	0.44	0.37	0.29	0.35	0.34	0.27	0.33	0.32	0.26	0.25	0.19	0.10
Std MCC	0.03	0.03	0.06	0.03	0.06	0.08	0.04	0.05	0.08	0.03	0.04	0.05
With transfer learning												
	5%	2.5%	1.25%	5%	2.5%	1.25%	5%	2.5%	1.25%	5%	2.5%	1.25%
Average MCC	—	0.40	0.35	—	0.29	0.24	—	0.27	0.23	—	0.21	0.17
Median MCC	—	0.40	0.36	—	0.29	0.25	—	0.28	0.24	—	0.22	0.16
Std MCC	—	0.04	0.05	—	0.04	0.07	—	0.05	0.07	—	0.03	0.03

TABLE II: **Compared performance for heatwave occurrence prediction with different data aggregation protocols.** Performance is reported in terms of averages, medians and std of MCC, obtained from 40 independent learnings, for the four different aggregation protocols, T_s -only, Z_g -only, Combined- T_sZ_g , Stacked- T_sZ_g , from right to left (see text for details), without (top) and with (bottom) transfer learning. This Table clearly shows that Stacked- T_sZ_g protocol combining surface temperature and geopotential heights, with transfer learning learning achieve the best forecasting performance, with MCC significantly above 0, around 0.4, for all the three heatwave levels and with a mild decrease with the intensity of the extreme events.

mechanisms. This further suggests that these cross-spatial dynamics are better exploited and revealed when the fields mixed and combined together from the first layer of the deep learning architecture layer (and thus from finest available spatial dynamics scales), as in aggregation protocol P4 (Stacked- T_sZ_g), rather than when processed independently and combined at the last (decision, and coarse scale) layer, as in aggregation protocol P3 (Combined- T_sZ_g).

Transfer learning. To quantify the benefits of using transfer learning, prediction performance are compared when the training is performed independently for the three anomaly levels (hence without transfer learning) against when the training is performed with initialization of the weights of the network for a given heatwave level using the network weights learned from the immediately lower heatwave level. The weights of the training for the 2.5% heatwave level are initialized with the weights learned at the 5% heatwave level (i.e., the weights learned after 10 epochs). In the same way, the weights of the training for the 1.25% heatwave level are initialized with the weights obtained at the end of the training for the 2.5% heatwave level (i.e., after 5 epochs). Prediction performance achieved in terms of MCC (averaged over the 40 independent learning), with the four protocols, with and without transfer learning, are compared in Table II. The runs performed without transfer learning systematically consisted in 10 epochs and the MCC presented in Table II is the

average of the best MCC obtained among these 10 epochs for each run. It indicates that heatwave prediction performance, in terms of increased (average or median) MCC, achieved with transfer learning are consistently either comparable or significantly above those obtained without transfer learning. Also, the standard deviations computed across independent trials are significantly reduced when using transfer learning, thus indicating a weaker sensitivity to weight initialization prior to training. These benefits are more pronounced for the rarest (1.25%) class of extreme events.

Further, Fig. 3 compares, for the aggregation protocols P3 (Combined- T_sZ_g) and P4 (Stacked- T_sZ_g), the training and testing performance with and without transfer learning; the performance is reported in terms of MCC as functions of the number of training epochs. Interestingly, it shows that aggregation protocol P3 (Combined- T_sZ_g) *learns* faster but *generalizes* less; hence it *overfits* data as compared to aggregation protocol P4 (Stacked- T_sZ_g). This thus confirms that protocol P4 (Stacked- T_sZ_g) performs better in heatwave prediction.

Also, and importantly, Fig. 3 suggests that the transfer learning procedure permits to obtain comparable or better performance, compared to without transfer and that such improved performance are obtained with a single epoch of training, as opposed to the 5 to 10 epochs needed to achieve convergence in performance without transfer learning. Transfer learning thus permits better performance obtained at

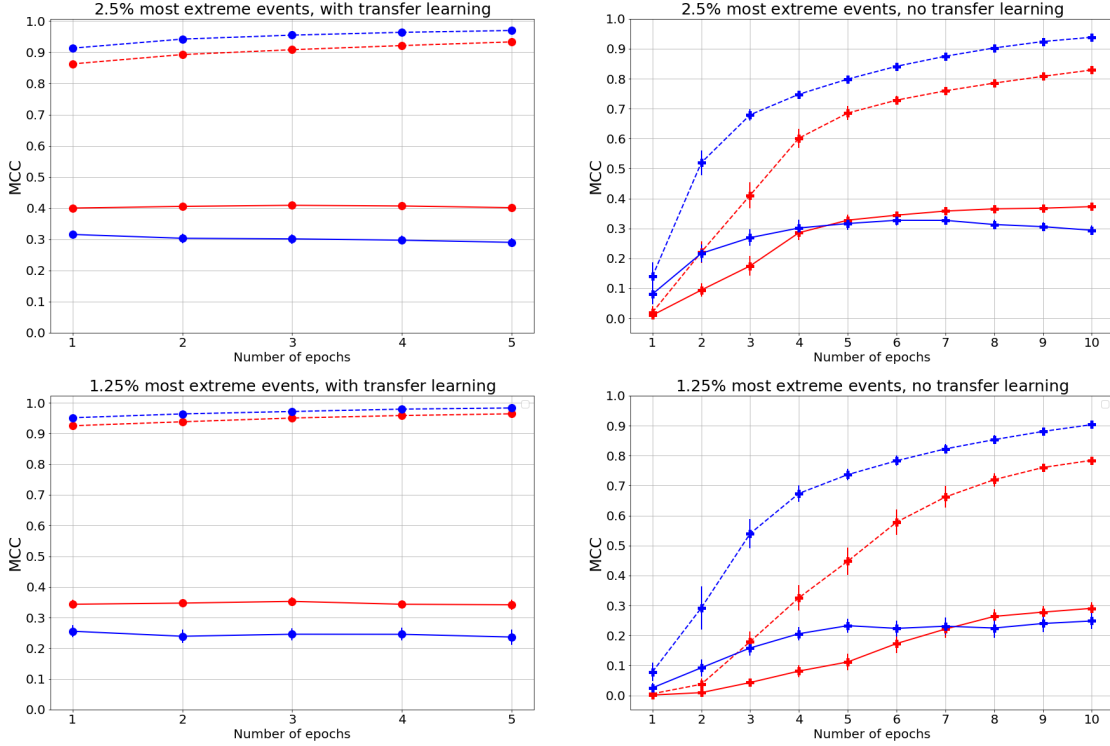


Fig. 3: **Forecasting performance in terms of MCC as a function of the number of epochs**, for aggregation protocols P3 (Combined- $T_s Z_g$) (blue) and P4 (Stacked- $T_s Z_g$) (red), without ('+', plots on the right) and with ('o', plots on the left) transfer learning. Solid (resp., dashed) lines correspond to testing (resp. training) performance. Top and bottom plots correspond respectively to the 2.5% and 1.25% most extreme events. Average MCC are obtained from 40 independent learning.

a significantly decreased computational cost.

Undersampling rate. In general, supervised learning (and a fortiori deep learning) for forecasting of extreme events faces potentially severe class imbalance. As described in Sec. III, it has been chosen to address this issue here by undersampling the large class of non extreme events. Table III compares achieved performance in terms of average MCC for different imbalance ratios between the non extreme and extreme class size, varying from 1 (equal class size), to 2, 4 and 10 and performance obtained with no undersampling. Table III shows that the undersampling strategy of the large non extreme event class during the training phase is effective as soon as it brings the training class-size imbalance to a ratio of 1 or 2, while performance degrades with larger ratios, 4 and 10, or no undersampling – hence large class-imbalance. This is particularly clear with transfer learning. To achieve optimal prediction performance, it is thus not mandatory that classes have exactly the same size but it is critical that class imbalance ratio remains limited of a few units.

For the sake of completeness, let us mention that the discussions above, related to data aggregation protocols and transfer learning, were presented with a class imbalance ratio

of $\simeq 2$ corresponding to sampling rate of $1/10$, $1/20$ and $1/40$ for the three levels of extreme events. Equivalent conclusions were drawn from analyzing results obtained with a class-size ratio of 1 corresponding to sampling rate of $1/19$, $1/39$ and $1/79$.

B. Forecasting performance

Heatwave prediction scheme. The methodological analyses reported above (cf. Table II) already yield the first key result of the present article: the occurrence of heatwaves, for the three levels of extreme events, within the next D days from present time t , can be predicted from data observed across space at the sole time t , and this for the four aggregation protocols.

Further, these analyses lead to choose to use the aggregation protocol P4 (Stacked- $T_s Z_g$), with transfer learning and non extreme event class undersampling rates of $1/10$, $1/20$ and $1/40$ for the three levels of heatwaves, as optimal. These findings permit to conduct a systematic analysis of prediction performance as functions of τ , the number of days in advance heatwaves have to be predicted: that is, surface temperature and geopotential height fields at date $t - 8 \times \tau$ are used to predict a heatwave occurring any time between dates t and $t + 8 \times D$.

No transfer learning	1, 1, 1			1/2, 1/4, 1/8			1/5, 1/10, 1/20			1/10, 1/20, 1/40			1/19, 1/39, 1/79		
Levels	5%	2.5%	1.25%	5%	2.5%	1.25%	5%	2.5%	1.25%	5%	2.5%	1.25%	5%	2.5%	1.25%
Average MCC	0.36	0.28	0.23	0.39	0.39	0.31	0.44	0.38	0.10	0.44	0.29	0.08	0.41	0.20	0.09
Median MCC	0.36	0.28	0.23	0.40	0.39	0.33	0.43	0.38	0.04	0.44	0.32	0.06	0.42	0.24	0.08
Std MCC	0.03	0.07	0.08	0.04	0.04	0.08	0.04	0.03	0.12	0.03	0.07	0.08	0.03	0.10	0.06
Transfer learning															
Average MCC	—	0.27	0.18	—	0.33	0.25	—	0.38	0.31	—	0.40	0.35	—	0.38	0.34
Median MCC	—	0.25	0.20	—	0.33	0.25	—	0.37	0.32	—	0.40	0.36	—	0.39	0.34
Std MCC	—	0.06	0.06	—	0.06	0.08	—	0.04	0.07	—	0.04	0.05	—	0.03	0.04

TABLE III: **Compared performance for heatwave occurrence prediction with different undersampling rates.** Performance is reported in terms of average, median and std MCC, obtained from 40 independent learning, for aggregation protocol P4 (Stacked- $T_s Z_g$) for the three levels of anomalies, without (top) and with (bottom) transfer learning, for no undersampling (left) to high undersampling (right). This table shows that the undersampling strategy of the large non extreme event class during the training phase is effective for an imbalance ratio of the order of two.

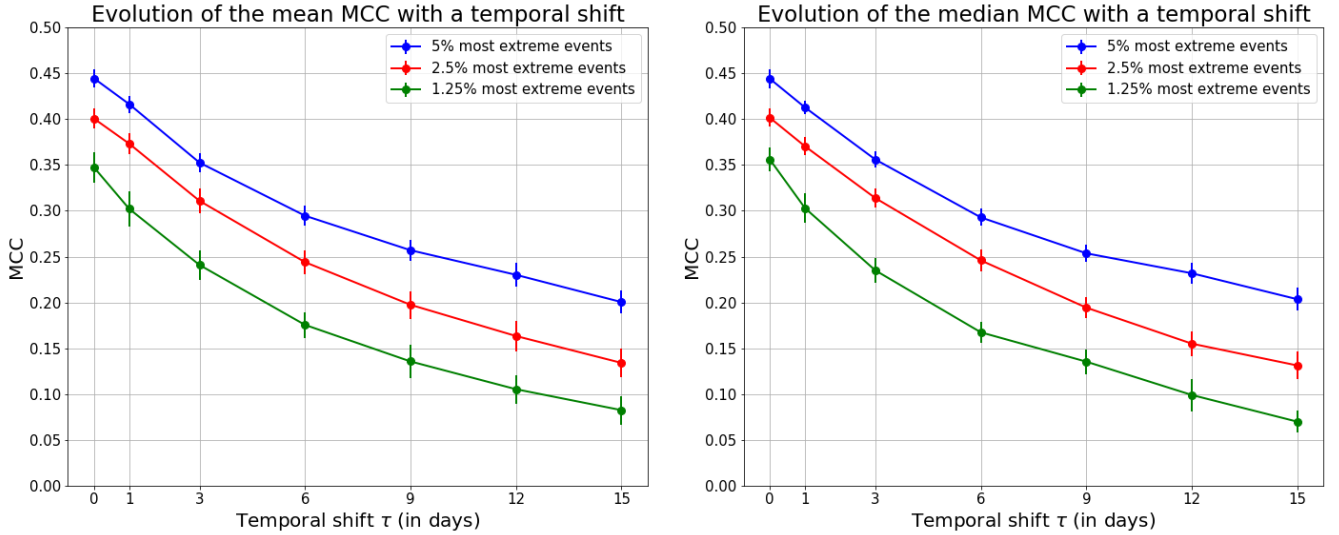


Fig. 4: **Heatwave occurrence prediction performance in MCC as function of the number of days in advance τ .** Mean MCC, with standard deviation, (left plot) and median MCC, with max absolute deviation, (right plot), obtained as averages across the 40 independent learning, for the three levels of extreme events. These plots clearly show that achieved MCC are significantly above 0 indicating the ability of the proposed Deep Learning procedure to predict heatwave extreme events τ days in advances from the sole observations of the surface temperature and geopotential height fields at a single date.

The training procedure is repeated 40 times from scratch with independent yearly-based train/test data split, as for $\tau = 0$ and as described in Section III.

Heatwave prediction performance. Fig. 4 reports, for the three level of extreme events, the means, \pm standard deviations (left), and medians \pm max absolute deviations (right), obtained as averages across the 40 independent learning, as functions of the prediction delay τ .

These plots demonstrate that the achieved MCC significantly depart positively from 0, and this for the three levels of extreme events and for $0 \leq \tau \leq 15$ days. They also show that the decrease in MCC as function of τ is slow, decreasing from the range 0.35 to 0.45 at $\tau = 0$ to the still significant range of 0.10 to 0.20 at $\tau = 15$, thus that occurrence prediction as early as 15 days in advance is achieved.

To complement these performance analyses, Fig. 5 reports the evolution, with respect to the prediction scale τ , of the True Positive and False Positives rates (i.e., respectively $TP/(TP + FN)$ and $FP/(FP + TN)$ in percentage). It shows that the

decrease in performance quantified by the decrease of MCC in Fig 3 stems from a decrease in the TP rate: While the prediction horizon τ increases, fewer heatwaves are detected. The False Positive Rate remains constant, and hence so does the number of FP, to less than 10% of the total number of negative samples: While the prediction horizon τ increases, the detection of negative events remains "as easy".

All together, achieved performance yield the following conclusions, consisting per se of relevant findings for climatologists:

i) The surface temperature and geopotential height spatial fields in North hemisphere at a single observation time contain sufficient spatial structures and information to predict the occurrence of heatwaves over European territory of the size of France, up to 15 days ahead of the beginning of a long lasting heat wave.

ii) Beyond independent spatial-dynamics, the cross-spatial dynamics of these two fields contain relevant structures permitting to enhance significantly prediction performance. The fact that the aggregation protocol P4 (Stacked- $T_s Z_g$) outperforms

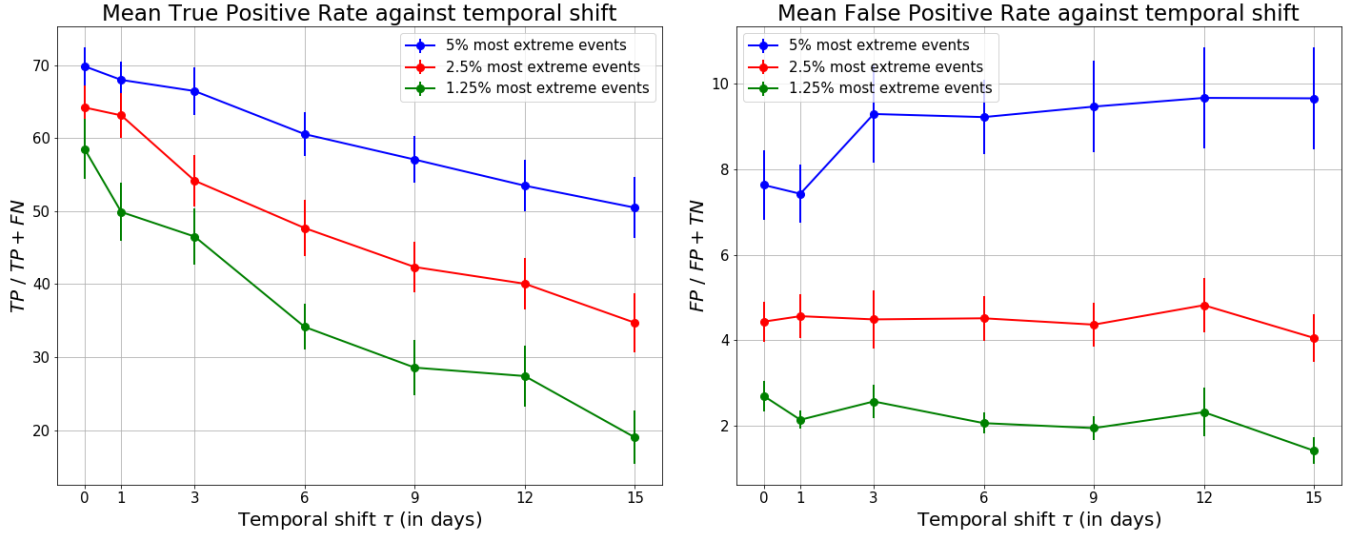


Fig. 5: **Compared performance for heatwave occurrence prediction as a function of τ .** Compared rates (in percentages) of True positive (left plot) and False positive (right plot) predictions, for each heatwave levels (5%, 2.5% and 1.25%). Average across 40 independent learning as described in Figure 3. Percentages of True Positives (resp. False Positives) are quantified with respect to the sizes of the positive (resp. negative) class.

other field combination strategies clearly indicates that such cross-dynamics must be processed jointly from the finest available physical scales.

iii) CNN-layer based Deep-Learning architectures prove able to extract relevant (cross-)spatial dynamics of climate data. Convolutional filter sizes were varied and results were reported here only for the best prediction performance, corresponding to filter size ranging from 9×9 to 12×12 . In physical units, this corresponds to filters exploring jointly frequency bands of width $\Delta f \sim 10^{-3} \text{ km}^{-1}$ and thus (cross-)spatial dynamics within territories of size roughly corresponding to $1000 \times 1000 \text{ km}^2$. Incidentally, this turns out to correspond to the size of a typical spatial correlation length, the order of magnitude of the size of cyclonic and anticyclonic anomalies, of the order of the Rossby deformation radius [14].

iv) Predicting heatwaves at $\tau = 0$ is already an impressive outcome, as it corresponds to predicting the occurrence of an extreme event, within the next $D = 14$ days from the observation of a extremely limited amount of climate data potentially available for prediction (2 spatial fields only at a single observation time). The ability of the proposed scheme to predict heatwaves as early as 15 days in advance is even more impressive. Indeed, typical correlation times in climate time series are documented to be of 3 to 5 days [14]. Predicting the occurrence of heatwaves 3 to 5 times ahead of that correlation time suggests that the proposed forecasting scheme has extracted relevant fine (cross-)spatial structures from data, a remarkable outcome.

V. CONCLUSIONS AND PERSPECTIVES

The present work has illustrated and quantified the ability of deep learning approaches to predict the forthcoming occurrence of climate extreme events, such as long-lasting heatwaves, from an extremely restricted subset of climate data.

One key result obtained here has been to show that significant prediction performance can be achieved from the analysis of the (cross-)spatial dynamics of only two fields observed at a single time point, and that prediction extends in time beyond typical climate correlation time scales.

These successes are grounded:

- i) on the use of a large size training database, consisting here in 1000 years of simulated climate data as well as the use of surface temperature and geopotential heights, chosen a priori as relevant information to heatwave dynamics from the existing scientific literature;
- ii) on the use of CNN-layer based neural network architectures;
- iii) on combining CNN with in-depths analyses of issues such as data aggregation, non extreme event large class undersampling to address class-size imbalance intrinsically associated with extreme-event predictions, transfer learning and nested extreme event structure to achieve relevant prediction of the most extreme events, using learning performed from less extreme events. The study and assessment of these three practical procedures can be seen as methodological contributions valid in generic settings and in other applications facing extreme event predictions and imbalanced class sizes.

At the application level, the claim is not that deep learning approaches should replace physics-driven models in climate predictions. Rather, the present work can be read as a proof of concept result for the use of learning procedure, and here a specific deep learning architecture, in climate extreme event predictions. At this stage, it mostly provides climatologist with a *black-box* tool that performs heatwave occurrence predictions with satisfactory performance, and at very low computational costs in time and computer resources and using very limited sets of observations. Achieving the same task with the traditional physics-model based approach requires

solving a set of dynamical partial differential equations in climate simulator engines, involving significant computational resources and observed data for initialisation.

This work will be continued along several lines.

On the application side, the extent to which aggregating other spatial fields available (e.g., several geopotential isolines) on the same day would improve prediction performance will be investigated. Also, it will be studied how combining observations made across several times, thus aggregating temporal and spatial dynamics in deep learning architectures, can be done to improve heatwave occurrence forecasting performance. Further, the prediction of shorter-duration heatwaves, or of heatwaves occurring on different areas will be analyzed.

At the methodological level, it would be natural to try to relate prediction performance to architecture complexity, which could be quantified using the Vapnik-Chervonenkis Dimension tool, as recently suggested and explored in [24], [25], [26]. It would also be useful to try to incorporate physics knowledge and interpretability of the trained neural network to contribute to the understanding of the physical mechanisms at work in heatwave dynamics.

REFERENCES

- [1] IPCC. *Climate Change 2013: The Physical Science Basis. Contribution of Working Group I to the Fifth Assessment Report of the Intergovernmental Panel on Climate Change*. Cambridge University Press, Cambridge, United Kingdom and New York, NY, USA, 2013.
- [2] R. García-Herrera, J. Díaz, R. M. Trigo, J. Luterbacher, and E. M. Fischer. A Review of the European Summer Heat Wave of 2003. *Critical Reviews in Environmental Science and Technology*, 40(4):267–306, 2010.
- [3] D. Barriopedro, E.M. Fischer, J. Luterbacher, R.M. Trigo, and R. García-Herrera. Redrawing the temperature record map of europe. *Science*, 332:220–224, 2011.
- [4] F. Otto, N. Massey, Geert Jan Van Oldenborgh, R. Jones, and M. Allen. Reconciling two approaches to attribution of the 2010 russian heat wave. *Geophysical Research Letters*, 39:4702–, 02 2012.
- [5] J.A. Weyn, D.R. Durran, and R. Caruana. Can machines learn to predict weather? using deep learning to predict gridded 500-hpa geopotential height from historical weather data. *Journal of Advances in Modeling Earth Systems*, 11(8):2680–2693, 2019.
- [6] P.D. Dueben and P. Bauer. Challenges and design choices for global weather and climate models based on machine learning. *Geoscientific Model Development*, 11(10):3999–4009, 2018.
- [7] S. Scher and G. Messori. Weather and climate forecasting with neural networks: using general circulation models (gcms) with different complexity as a study ground. *Geoscientific Model Development*, 12(7):2797–2809, 2019.
- [8] T. Schneider, S. Lan, A. Stuart, and J. Teixeira. Earth system modeling 2.0: A blueprint for models that learn from observations and targeted high-resolution simulations. *Geophysical Research Letters*, 44(24):12–396, 2017.
- [9] N.D. Brenowitz and C.S. Bretherton. Prognostic validation of a neural network unified physics parameterization. *Geophysical Research Letters*, 45(12):6289–6298, 2018.
- [10] P. Gentile, M. Pritchard, S. Rasp, G. Reinaudi, and G. Yacalis. Could machine learning break the convection parameterization deadlock? *Geophysical Research Letters*, 45(11):5742–5751, 2018.
- [11] Y. Liu, E. Racach, J. Correa, A. Khosrowshahi, D. Lavers, K. Kunkel, M. Wehner, W. Collins, et al. Application of deep convolutional neural networks for detecting extreme weather in climate datasets. *arXiv preprint arXiv:1605.01156*, 2016.
- [12] A. Chattopadhyay, E. Nabizadeh, and P. Hassanzadeh. Analog forecasting of extreme-causing weather patterns using deep learning. *Journal of Advances in Modeling Earth Systems*, 12(2), 2020.
- [13] A. McGovern, K.L. Elmore, D.J. Gagne, S.E. Haupt, C.D. Karstens, R. Lagerquist, T. Smith, and J.K. Williams. Using artificial intelligence to improve real-time decision-making for high-impact weather. *Bulletin of the American Meteorological Society*, 98(10):2073–2090, 2017.
- [14] Geoffrey K Vallis. *Atmospheric and oceanic fluid dynamics*. Cambridge University Press, 2017.
- [15] K. Fraedrich, H. Jansen, E. Kirk, U. Luksch, and F. Lunkeit. The Planet Simulator: Towards a user friendly model. *Meteorologische Zeitschrift*, 14(3):299–304, June 2005.
- [16] K. Fraedrich, E. Kirk, and F. Lunkeit. *PUMA: Portable University Model of the Atmosphere*. Technical report, Deutsches Klimarechenzentrum, Hamburg, 1998.
- [17] F. Ragone, J. Wouters, and F. Bouchet. Computation of extreme heat waves in climate models using a large deviation algorithm. *Proceedings of the National Academy of Sciences*, 115(1):24–29, 2018.
- [18] Ian Goodfellow, Yoshua Bengio, and Aaron Courville. *Deep Learning*. MIT Press, 2016. <http://www.deeplearningbook.org>.
- [19] B. Krawczyk. Learning from imbalanced data: open challenges and future directions. *Progress in Artificial Intelligence*, 5(4):568–572, 2016.
- [20] J.M. Johnson and T.M. Khoshgoftaar. The effects of data sampling with deep learning and highly imbalanced big data. *Information Systems Frontiers*, (22):1113–1131, 2020.
- [21] X. Glorot and Y. Bengio. Understanding the difficulty of training deep feedforward neural networks. In Yee Whye Teh and Mike Titterton, editors, *Proceedings of the Thirteenth International Conference on Artificial Intelligence and Statistics*, volume 9 of *Proceedings of Machine Learning Research*, pages 249–256, Chia Laguna Resort, Sardinia, Italy, 13–15 May 2010. JMLR Workshop and Conference Proceedings.
- [22] L. Y. Pratt. Discriminability-based transfer between neural networks. *Advances in Neural Information Processing Systems*, 5:204–211, 1993.
- [23] B.W. Matthews. Comparison of the predicted and observed secondary structure of t4 phage lysozyme. *Biochimica et Biophysica Acta (BBA) - Protein Structure*, 405(2):442 – 451, 1975.
- [24] Eric B Baum and David Haussler. What size net gives valid generalization? In *Adv Neural Inf Proc Systems*, pages 81–90, 1989.
- [25] Gerald Friedland and Mario Krell. A capacity scaling law for artificial neural networks. *arXiv preprint arXiv:1708.06019*, 2017.
- [26] P Liotet, P Abry, R Leonarduzzi, M Senneret, L Jaffrès, and G Perrin. Deep learning abilities to classify intricate variations in temporal dynamics of multivariate time series. In *ICASSP 2020-2020 IEEE International Conference on Acoustics, Speech and Signal Processing (ICASSP)*, pages 3857–3861. IEEE, 2020.
- [27] S. Ioffe and C. Szegedy. Batch normalization: Accelerating deep network training by reducing internal covariate shift, 2015.
- [28] J. Tompson, R. Goroshin, A. Jain, Y. LeCun, and C. Bregler. Efficient object localization using convolutional networks, 2014.
- [29] D. Lucente, S. Duffner, C. Herbert, J. Rolland, and F. Bouchet. Machine learning of committor functions for predicting high impact climate events. 10 2019.
- [30] D.J.C. MacKay. *Information Theory, Inference & Learning Algorithms*. Cambridge University Press, USA, 2002.
- [31] S. Scher. Toward data-driven weather and climate forecasting: Approximating a simple general circulation model with deep learning. *Geophysical Research Letters*, 45(22):12–616, 2018.
- [32] Y.-G. Ham, J.-H. Kim, and J.-J. Luo. Deep learning for multi-year ENSO forecasts. *Nature*, 573(7775):568–572, 2019.
- [33] IPCC. *Managing the risks of extreme events and disasters to advance climate change adaptation: special report of the Intergovernmental Panel on Climate Change*. Cambridge University Press, New York, NY, 2012.
- [34] S. Coumou, D. and Rahmstorf. A decade of weather extremes. *Nature Climate Change*, 2(7):491–496, 2012.